# Train speed calculation using ground vibrations

# Train speed calculation using ground vibrations

Georges Kouroussis[1], David P. Connolly[2], Mike C. Forde[3], Olivier Verlinden[1]

1. Université de Mons – UMONS, Faculty of Engineering,
Department of Theoretical Mechanics, Dynamics and Vibrations,
Place du Parc, 20 — 7000 Mons (BELGIUM)
2. Heriot-Watt University, School of the Built Environment,
Institute for Infrastructure and Environment,
Edinburgh EH14 4AS (UNITED KINGDOM)
3. University of Edinburgh, School of Engineering,
Institute for Infrastructure and Environment,
Edinburgh EH9 3JF (UNITED KINGDOM)
e-mail: georges.kouroussis@umons.ac.be

## Abstract

This paper presents a high precision train speed calculation technique based on ground vibration information. This versatile method can calculate speeds for trams, intercity locomotives and high speed trains on any track/embankment arrangement. Additionally, it has high accuracy for sensors located up to 100 m from the track, thus allowing semi-remote, non-invasive monitoring of train velocities. The calculation method combines three separate speed calculation techniques to provide estimates for arbitrary train speeds, even for sensors placed at large track offsets. The first estimation technique involves the use of cepstral analysis to isolate key harmonics for use with speed calculation. The second method is similar however the combination of a running *rms* and a previously developed "dominant frequency method" are used. The third method uses an analytical vibration frequency prediction model in combination with regression analysis to calculate train speed. All three methods are combined into one calculation procedure, resulting in high accuracy estimates. To show the robustness and ability of the new method to calculate a wide range of train speeds, it is used to predict tram, intercity and high speed rail train passage velocities generated from a previously validated vibration prediction numerical model. More importantly, it is used to predict train speeds during field trials performed on operational railway lines in Belgium and in UK. The new method is shown to have offer high performance for several train types and track setups (including abutment and tunnel cases).

## keywords

Railway ground vibrations; train speed; excitation passage mechanisms; vehicle–track dynamics; high speed rail; intercity; tramway; velocity measurement

# 1 Introduction

## 1.1 Conventional train speed calculation

Evaluating railway vehicle speed is of growing interest for both railway operators and researchers working in the area of noise and vibration assessment. For researchers, the relationship between train speed $v_0$ and vibration magnitude has generated significant interest, whereas for railway operators it is important to monitor speeds across the network. Existing methods for evaluating the vehicle speed are subject to shortcomings, particularly after the European Union imposed a domestic separation between railway operators and transport infrastructure operators. In Belgium, Infrabel operates the railway network and the primary rolling stock manager is SCNB/NMBS (for Société de Chemin de fer Nationale Belge/Nationale Maatschappij der Belgische Spoorwegen).

A brief description of the most commonly used methodologies for monitoring the train speed is:

- **Tachometer**: This information comes from the vehicle driver who has access to the speedometer. Two drawbacks are associated with this method. Firstly it is difficult to accurately determine the speed at the exact measurement location and secondly it requires additional infrastructure to ensure reliable communication with the rolling stock manager.
- **GPS**: A global positioning system is analogous to the tachometer however it provides a more accurate estimation of the vehicle location. Despite this, for a large number of events (for example, the measurement of ground vibrations on all trains across a rail network), the cost can be prohibitive.
- **Radar**: Radar uses the Doppler effect to calculate speed. Precision is very high if the equipment is accurately positioned (near the track and exactly parallel to the rail).
- **Camera**: If the railway landscape permits it, the use of a camera recorder (i.e. at-grade track or small backfill embankment) at a large distance from the track, can be used to calculate the vehicle speed, based on the movie frame count. Fixed objects on the video are necessary, as for example the portal catenary supports of the railroad line (Fig. 1). Camera recorder can be also used for capturing the arrival of the train to the vibration sensors [1].

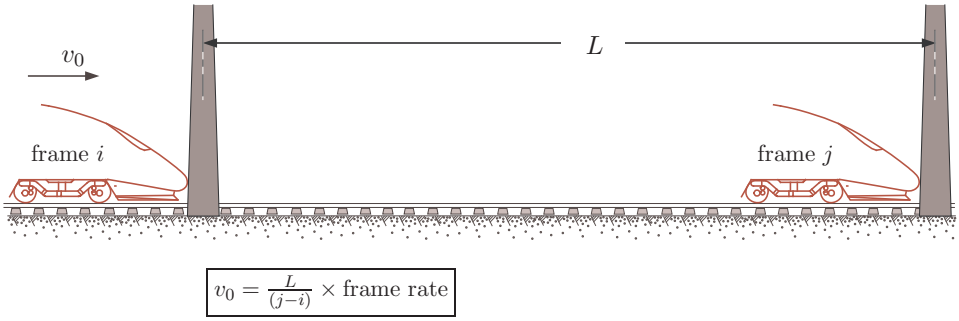


Figure 1: Speed evaluation based on the use of a camera recorder placed at a large distance from the track

- **Wheel counters**: Wheel counters are sensors that are fixed to the rail and detect the passage of train wheels. They are commonly used to calculate train speed however their installation requires direct track access. This access can be difficult to obtain, especially for untrained persons due to safety legislation. Additionally, depending on this legislation, track closure may be required for installation. Although the accuracy of wheel counters is high, these installation challenges make them relatively static in nature and difficult to adapt to changes in requirements. Therefore, if numerous measurements are required along a line or if speed measurements are only needed over a short time period, the time required for installation, removal and transportation may make them undesirable.

- **Optical sensors**: The optical photoelectric sensing method, as proposed by [2], is a direct and accurate way to evaluate the train speed in-situ. A transmitter and a receiver are placed on both sides of the track, allowing detecting the passing of the vehicle using a light beam. The knowledge of the train length and the time needed to pass the sensor is used to calculate the speed. The use of a second identical system, placed at a sufficient distance along the track, improves accuracy (Fig. 2). A variant of this method uses vibration sensors instead of optic devices: by placing also two sensors at a sufficient distance $L$ along the track and measuring the vibrations during the passing of the train with a data recorder equipped with synchronisation timing, the speed can be evaluated knowing the time delay $\tau$ between the two recorded signals (Fig. 3). This method has been used in conjunction with a camera by [3] for high-speed train (HST) measurement.

Table 1 summarizes these different methods with an emphasis on the advantages, disadvantages, and the accuracy of each method.

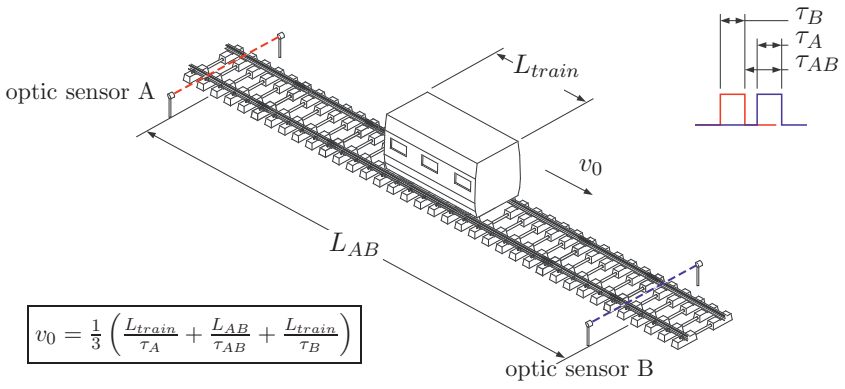


Figure 2: Speed evaluation based on two optical sensors placed along the track

## 1.2 Vibration-based evaluation with the help of the dominant frequencies

A new approach to train speed calculation using on ground vibration measurements was been proposed by [2]. This non-conventional approach has seldomly been used in practise however it provides an attractive alternative to the aforementioned conventional methods. The approach was based upon analysing dominant frequencies. [4–7] have shown that ground vibration railway frequency spectra are highly dependent on train speed and coach dimensions. Furthermore, Ju et

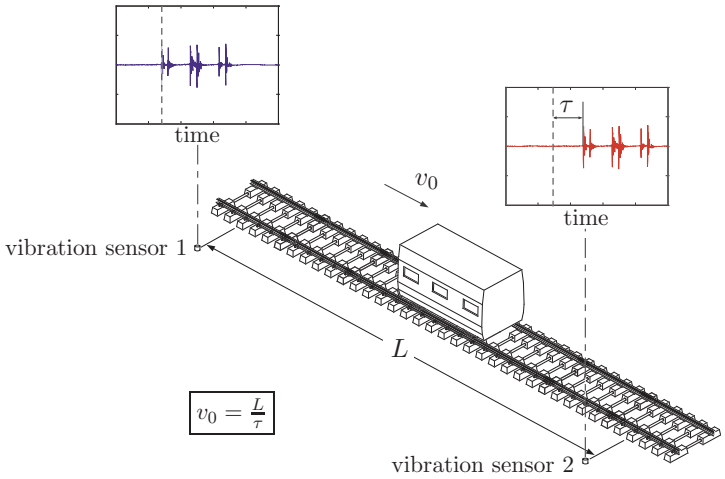


Figure 3: Speed evaluation based on two vibration sensors placed along the track

Table 1: Existing conventional methods for evaluating vehicle speed

| **Method** | **Physical phenomenon** | **Advantage** | **Drawback** | **Error** |
|---|---|---|---|---|
| camera | frame-counter | accessible device | track view access | depending on the camera resolution |
| GPS | geolocalisation | cheap | using inside the train | from 5 to 10% |
| optic sensors | optic | very accurate | track access | $< 1\%$ |
| tachometer | revolution-counter | no additional measurement | administrative procedure | 5% |
| radar | Doppler effect | Easy to use | accuracy depending on the position | from 1 to 5% |
| wheel counter | contact | very accurate | track access | $< 1\%$ |

al. [8] investigated the characteristics of ground vibrations in the frequency domain by analysing the dominant frequencies induced by trainloads. Then, Ni et al. [2] proposed an a posteriori numerical method for train speed calculation based on ground vibration measurement. This automatic procedure was based on the isolation of the dominant excitation frequencies at

$$f_{c,n} = n\frac{v_0}{L_c} \qquad (n = 1, 2, 3, \dots) \tag{1}$$

where $L_c$ was the coaches length.

The approach required the user to define a frequency range $[f_{c,1,\text{lower}}; f_{c,1,\text{upper}}]$, within which the maximum amplitude of the fundamental frequency $f_{c,1}$ was found. Then a recursive calculation of the $n^{th}$ dominant frequency $f_{c,n}$ was performed by finding the maximum in the frequency

range:

$$[f_{c,n,\text{lower}};f_{c,n,\text{upper}}] = [(n-0.45)\times f_{c,avg};(n+0.45)\times f_{c,avg}] \tag{2}$$

where $f_{c,avg}$ represented the average of the fundamental frequency, calculated by

$$f_{c,avg} = \begin{cases} f_{c,1} & \text{if } n=2 \\ \dfrac{1}{n-1}\displaystyle\sum_{i=1}^{n-1}\frac{f_{c,i}}{i} & \text{if } n>2 \end{cases} \tag{3}$$

as proposed by the authors. For each dominant excitation frequency $f_{c,n}$, the train speed was estimated using

$$v_{0,n} = \frac{f_{c,n}L_c}{n} \tag{4}$$

and the final train speed was given by

$$v_0 = \min_n(v_{0,n+1} - v_{0,n}) \ . \tag{5}$$

A safeguard was implemented in order to reject some poorly-estimated dominant excitation frequencies $f_{c,n}$ which did not satisfy the criterion

$$\left|\frac{f_{c,n}}{n} - f_{c,1}\right| = 0.3\ f_{c,1} \ . \tag{6}$$

Additionally, $n$ was limited to 10 due to the decrease of amplitude with the distance (soil material damping). The authors validated their method by calculating HST passage speeds, verified using experimental results from optical sensors, for speeds in the range 200–300 km/h. They postulated that the dominant frequency method was more convenient, mobile and economical than traditional methods. In the case of ground vibration assessment, no additional device was needed.

This procedure had advantages over other methods however suffered from several shortcomings:

- All calculations were based on the evaluation of the fundamental dominant excitation frequency $f_{c,1}$. Therefore a poor estimation of this value could prevent divergence in the calculation of vehicle speed.
- The calculation of the maximum for each frequency range defined by Eq. (2) could be subject to errors if the signal contained strong excitations from sources other than from the vehicle periodicity (e.g. vehicle natural frequency). As part of this research, the dominant frequency method was tested and was found to yield vastly different speed estimates depending on the sensor distances from the railway line. This was caused by strong soil resonance frequencies.
- The value of 0.3 used in Eq. (6) was arbitrarily chosen by Ni et al. and was likely based on the site specific high-speed train data used for testing the method. Therefore, it had no scientific basis and could fail under certain circumstances (e.g. freight trains, different soil conditions,...).

### 1.3 Paper Outline

This paper presents a new train speed calculation method based upon the fundamental principles outlined by Ni et al. Two completely new ways are developed to calculate train speed and are combined with Ni's method. These methods are based on cepstral analysis and analytical/regression technique respectively. The aim was to overcome the shortcomings and extend the domain of validity of current methods After a brief review of the source of ground vibrations, a new procedure for train speed calculation is presented. The new approach is found to have several significant benefits over other approaches. Then the effectiveness of the new method and its ability to predict a wide spectrum of train speeds are shown. Finally, Practical results are presented, based on numerical and experimental data. It should be noted that vehicle speed is assumed to be constant in this work.

## 2 Analytical calculation of railway-induced excitation frequencies

The vehicle, the track and the soil, play different roles in the generation of ground vibrations. In an attempt to categorize the frequency bands associated with these components, Alias [9] proposed that they could be divided into frequency ranges with limits not well defined:

- Vehicle dynamics dominate the low-frequency range (until 15 Hz) and are efficiently transmitted to the ground if significant defects in the wheel/rail contact excite the vehicle natural modes.
- Mid range frequencies (from 15 Hz to 150 Hz) are due to track components (and track flexibility) with possible amplification due to the soil resonance.
- High-frequencies (over 150 Hz) constitute rolling noise and are due to wheel/rail sliding. They rarely intervene in the ground vibrations because the soil strongly attenuates the vibrations (material and geometrical damping).

Regarding the soil, Kouroussis et al. [10] attempted to quantify the effect of vehicle and track parameters on ground vibrations levels. It was also found that the soils Young's modulus and damping characteristics had a significant effect on vibration levels [11].

### 2.1 Train and track response calculation

Knowledge of amplitude modulation and key excitation frequencies makes it more straightforward to understand the generation and propagation of ground waves. Once these characteristics are understood then it became possible to utilise them for train speed calculation purposes. Calculation of the vertical deflection $w(x,t)$ of the track subjected to a load $P_{wheel}$ moving at a constant speed $v_0$ was assumed to be a problem that could be solved using traditional beam theory (Fig. 4). Euler–Bernoulli beam theory was used to represent the behaviour of the track

$$E_r I_r \frac{\partial^4 w}{\partial x^4} + K_f w = P_{wheel}\delta(x - v_0 t) \tag{7}$$

where the track (two parallel rails with periodically fastened sleepers) was approximated as an elastic beam (Young modulus $E_r$, cross-sectional momentum $I_r$, section $A_r$, density $\rho_r$). The

beam was assumed to be lying on a Winkler's foundation, defined by its stiffness $K_f$ per unit of length, including railpad and ballast contributions. This parameter was approximated by

$$K_f = \left( \frac{L}{k_b} + \frac{L}{k_p} \right)^{-1} \tag{8}$$

from the ballast $k_b$ and railpad $k_p$ stiffnesses, and the sleepers spacing $L$. The track was considered massless. This was a valid assumption for train speeds below the critical track/soil velocity, because quasi-static effects dominate the track response. The solution of Eq. (7) therefore could be written as

$$w(x,t) = w(x - v_0 t) = \frac{P_{wheel}}{8 E_r I_r \beta^3} \mathrm{e}^{-\beta |x - v_0 t|} \left[ \cos(\beta |x - v_0 t|) + \sin(\beta |x - v_0 t|) \right] \tag{9}$$

where $\beta = \sqrt[4]{\frac{K_f}{4 E_r I_r}}$.

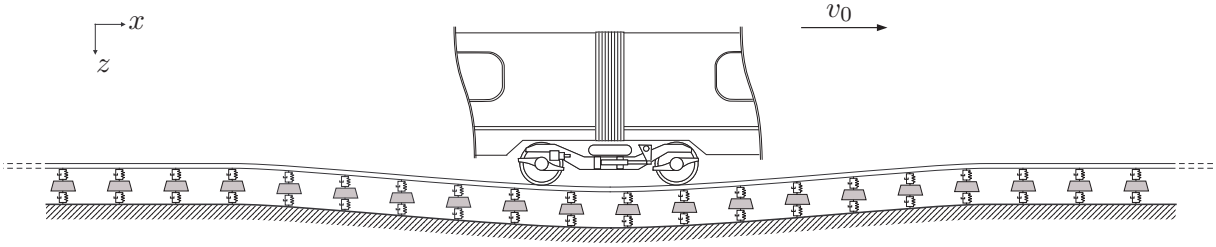


Figure 4: Vehicle moving on a flexible track

Figure 5 (solid line) illustrates the solution for the passage of a single wheelset from a HST, calculated using Eq. (9). Frequency content is shown in Fig. 5(b) to illustrate how vibration magnitude decreases with the frequency. The cut-off frequency depends on $\beta$ as increasing $\beta$ results in the cut-off frequency becoming more dominant. It also induces a large frequency range where the magnitude is constant (in engineering terms, the cut-off frequency is proportional to the foundation stiffness because the dynamic characteristics of the rail are relatively constant). A similar effect can be observed with speed. In the time domain, as speed $v_0$ increases, the rail deflection tends to an impulse Dirac delta (in the spatial domain, this effect is negligible).

When more than one wheelset is considered in the track deflection calculation, the effect of bogie spacing $L_b$ or the carriage length $L_c$ intervenes (Fig. 6). Figure 5 (dashed line) repeats the previous results for the case of a two wheel bogie configuration (as illustrated in Fig. 4). Amplitude modulation is observable due to the fundamental axle passage frequency $f_a = \frac{v_0}{L_a}$ at regular frequency intervals with zero amplitude at frequencies $\frac{2k+1}{2} f_a$ ($k \in \mathbb{N}$). A second amplitude modulation is apparent for a entire carbody (Fig. 5 — dash-dot line). This phenomenon can be repeated with the periodicity of the carbody of the vehicle, with dominant frequencies defined by Eq. (1) where the maximum amplitudes follow the carriage envelope. It should be noted that some dominant frequencies are suppressed if $L_c$ is a multiple of $L_a$ (rarely the case for $L_b$). Additionally, conventional HST's use a Jacobs bogie configuration where the carriage bogies are placed half under one car and half under the next. This leads to $L_b = L_c$; otherwise, a third modulation is observed. To illustrate this, theoretical rail deflections are presented in Figs. 7 and 8, taking into account the number of carriages for a Thalys HST and a conventional

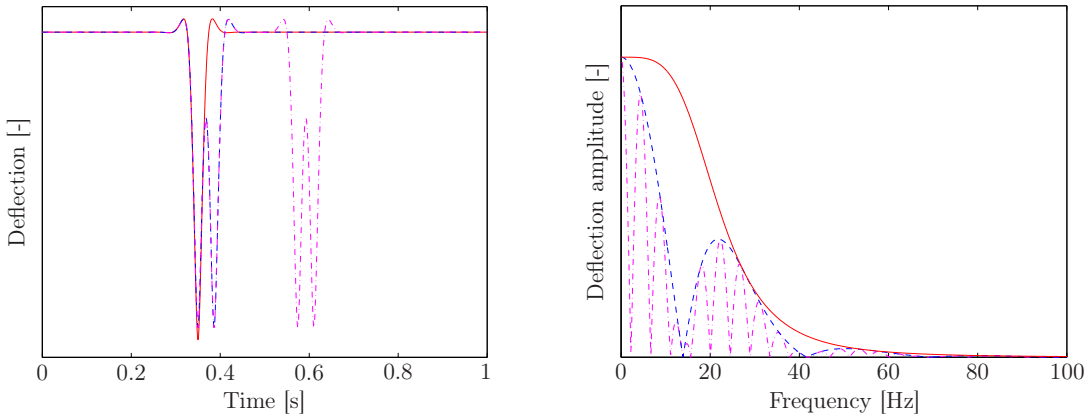


(a) Time history (b) Frequency content

Figure 5: Rail deflection due to the moving of a HST vehicle ($L_a = 3\,\text{m}$, $L_b = 18.7\,\text{m}$) at speed $v_0 = 300\,\text{km/h}$ (solid line: single wheelset; dash line: single bogie; dash-dot line: entire carbody)

domestic train, respectively. In the second case, the peaks are not located at the lobe maxima frequencies.

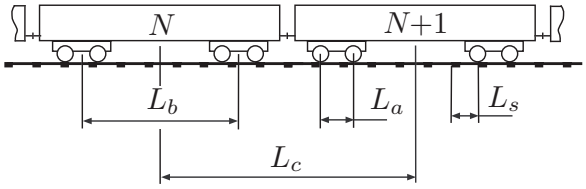


Figure 6: Main geometrical parameters of the train and the track

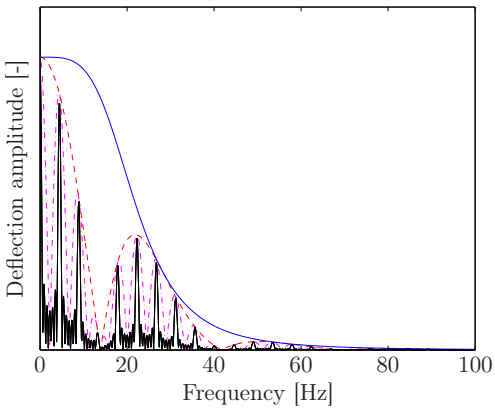


Figure 7: Frequency content calculated from the rail deflection due to the moving of a HST vehicle (8 carriages with $L_b = 18.7\,\text{m}$ and $L_a = 3\,\text{m}$) at speed $v_0 = 300\,\text{km/h}$

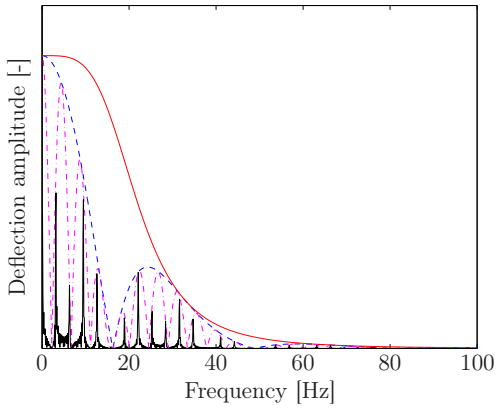


Figure 8: Frequency content calculated from the rail deflection due to the moving of an AM96 vehicle (3 carriages with $L_c = 26.4\,\text{m}$, $L_b = 18.7\,\text{m}$, $L_a = 2.56\,\text{m}$) at speed $v_0 = 150\,\text{km/h}$

## 2.2 Soil response calculation

As railway traffic generates ground vibration waves which induce small material deformations (shear strain is smaller than $10^{-5}$ in most practical cases), the soil is considered as a linear medium and can satisfy the superposition principle. The same dominant frequencies intervene in the ground vibration spectra with various added phenomenons:

- The vehicle dynamics can amplify the spectrum at low frequencies by adding some peaks and/or amplifying the excitation passages frequencies.
- The ground presents two kind of attenuation: geometric damping and material soil damping. This implies the exponential decrease of vibration magnitude with distance and an attenuation at high-frequencies respectively. Moreover, if the ground is considered as a superposition of layers with different dynamic properties, a resonance can appear if the difference in rigidity between the two top layers is significant and the excitation acts in the vertical direction [11]. The corresponding frequency can be approximated by [12]

$$f_{soil} = \frac{c_P}{4\,h} \tag{10}$$

  with $c_P$ the longitudinal wave velocity and $h$ the depth of the soil first layer. Practically, this resonance occurs in a frequency range between 20 and 60 Hz according to the site configuration. Notice that, for a layered ground with rigidity increasing with the depth, a low percentage of energy is transmitted below this cut-off frequency, attenuating the excitation frequencies in this area [11].
- Track dynamics have a negligible influence in the frequency range of interest, except a first resonance frequency where the rail and sleepers vibrate vertically in phase (typically around 60–150 Hz). Sleeper excitation passage frequency is also defined as

$$f_s = \frac{v_0}{L_s} \tag{11}$$

  and appear at high-frequencies (if the vehicle speed $v_0$ is greater than 100 km/h, $f_s$ is above 40 Hz, the sleeper bay $L_s$ being typically equal to 0.6 or 0.7 m).

The key train, track and soil excitation frequencies are illustrated in Fig. 9 which defines the frequency range of interest, according to [10, 12–14].

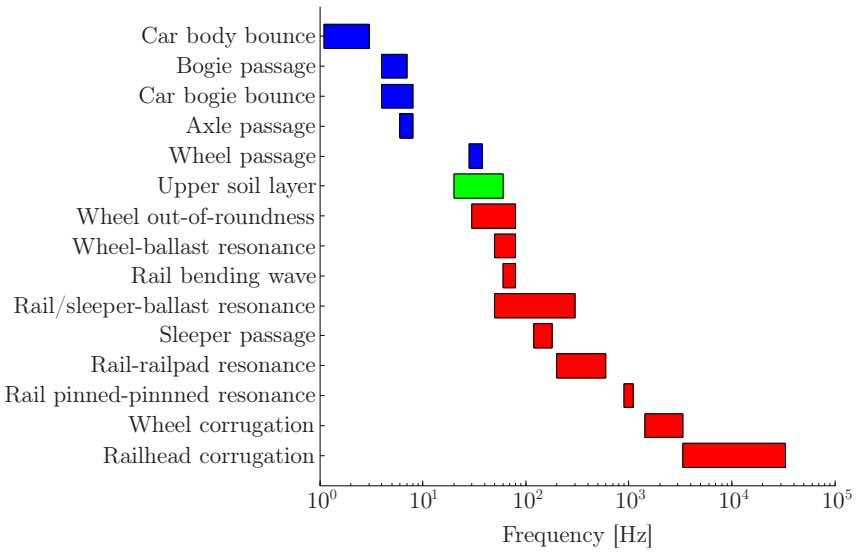


Figure 9: Main contribution of dynamic vehicle/track and soil interactions

# 3 The new train speed prediction method

## 3.1 Enhancing vehicle speed estimation

### 3.1.1 The use of cepstral analysis

As shown previously, the frequency spectrum amplitudes $V_i(f)$ of measured ground vibrations $v_i(t)$ contain important information related to the characteristics of the train passage. To extract this information, cepstral analysis can be used. This facilitates the determination of the periodicity of a numerical signal. A cepstrum is defined as the Fourier transform of a logarithmic spectrum and commonly known as the "spectrum of a spectrum" where

$$C_v(\tau) = \text{iDFT}\left(\log\left|V_i(f)\right|\right) \ . \tag{12}$$

A cepstrum is a function of quefrency $\tau$, numerically obtained using the inverse discrete Fourier transform (iDTF). The quefrency of the cepstrum peaks represents the modulation period, and its reciprocal, the modulating frequency. Note that, $x$, $y$ or $z$ for horizontal parallel to the track, horizontal perpendicular to the track or vertical, respectively.

The advantage of using cepstral analysis rather than frequency analysis is that it makes families of uniformly spaced components in the spectrum, namely families of harmonics and sidebands, much more evident [15]. Therefore the final transform is able to reveal and quantify $1/f_c$ (harmonic) and $1/f_a$ and $1/f_b$ (sidebands) more efficiently. Figure 10 illustrates the method in the case of a conventional train, with dimensions ($L_c = 26.4\,\text{m}$; $L_b = 18.7\,\text{m}$; $L_a = 2.56\,\text{m}$) according to Fig. 6. As mentioned previously, $L_b = L_c$ is the case for HST's and only two excitation frequencies are apparent — the bogie wheelset periodicity and the carriage periodicity.

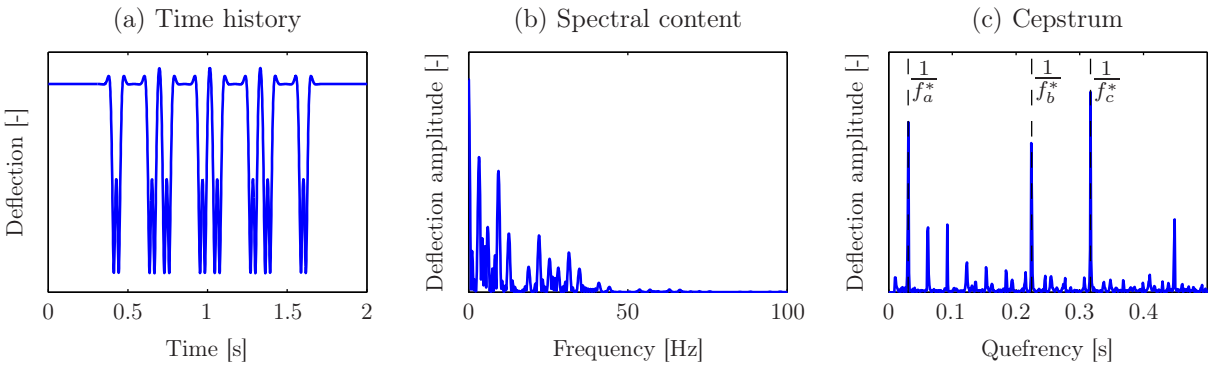


Figure 10: Application of the cepstral analysis to the track deflection corresponding to the passing of a conventional train (4-carriages) running at speed $v_0 = 300\,\mathrm{km/h}$

In some cases, cepstral analysis cannot replace the aforementioned dominant frequency method because the cepstral transformation can be negatively affected by external factors (e.g. additional excitation mechanisms and signal noise). However, it does provide a strong estimation of the fundamental frequency (or the starting frequency range for use with Eq. (2)) by

$$f_{c,1} = \frac{v_0^*}{L_c} \tag{13}$$

with $v_0^*$ the train speed evaluated as

$$v_0^* = \frac{1}{3}\left(L_c f_c^* + L_b f_b^* + L_a f_a^*\right) \tag{14}$$

where the cepstral characteristics $f_a^*$, $f_b^*$ and $f_c^*$ correspond to the excitation frequency associated with the wheelset periodicity, the bogie periodicity and the carriage periodicity, respectively (Fig. 10(c)).

### 3.1.2 The use of running *rms*

For exposures to vibration containing transient events, the running *rms* may be used in addition to the original signal. The running *rms* is calculated for a short integration time $t$ ending at time $t_0$ in the time record as follows

$$v_{rms,\tau}(t_0) = \sqrt{\frac{1}{\tau}\int_{t_0-\tau}^{t_0} v^2(t) e^{\frac{t-t_0}{\tau}} \mathrm{d}t} \tag{15}$$

where $\tau$ is the integration constant. This form of metric is typically used for human comfort evaluation through the DIN weighted vibrations severity $KB_F$ [16]. Figure 11 illustrates the applicability of the running *rms* for ground vibration measurements related to the passing of a Thalys HST at speed $v_0 = 300\,\mathrm{km/h}$. The integration constant $\tau$ is imposed sufficiently small (0.01 s) to smooth the original signal in order to fully resolve the carriage periodicity. This makes the passing passage of each wheelset clearer, thus highlighting the advantage of working with the running *rms* instead of the original vibration signal. Notice that these curves reveal different carriage periodicities due to the presence of conventional locomotives and side carriages on both

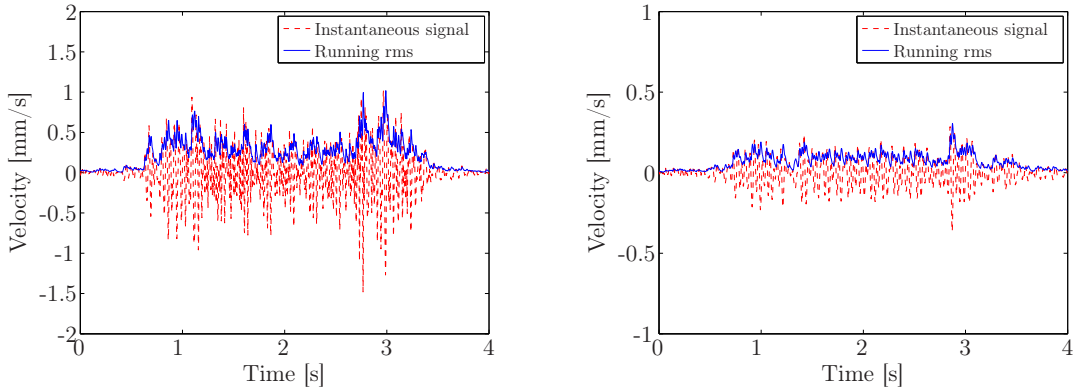


(a) Near field vibrations (b) Far field vibrations

Figure 11: Comparison between a time history and running $rms$ ($\tau = 0.01\,\mathrm{s}$) in the case of a Thalys HST running at speed $v_0 = 300\,\mathrm{km/h}$

extremities of the HST. Despite this, the effect is negligible compared to the larger number of central carriages (8).

Figure 12 compares the spectral characteristics of the original signal shown in Fig. 11 and the corresponding running $rms$, by varying the integration constant. Several carriage passage harmonic frequencies have become evident. The effect of the integration constant variation is also clear, showing that a value of $\tau = 0.01\,\mathrm{s}$ is a good choice. Notice that some frequencies are attenuated between 20 and 30 Hz, corresponding to the soil resonance amplification.

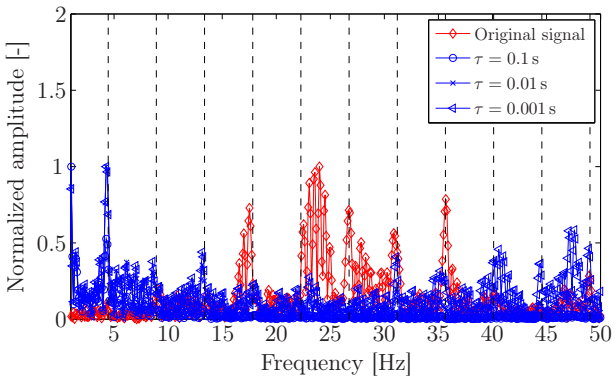


Figure 12: Spectral amplitude of running $rms$ in the case of a Thalys HST running at speed $v_0 = 300\,\mathrm{km/h}$

### 3.1.3 Regression analysis

A limitation of the dominant frequency method arises from the sampling operation during the analogue-digital conversion. This occurs because the vibration signal is recorded during a limited time period $T$. The use of a discrete Fourier transform (or another discrete-time Fourier estimation) implies that the spectrum is available only at discrete frequencies $k\Delta f$ ($k = 0, 1, 2, \dots$)

and the speed resolution $\Delta v_{0,n}$ depends on these considerations:

$$\Delta f = \frac{1}{T} \quad \Leftrightarrow \quad \Delta v_{0,n} = \frac{L_c \Delta f}{n} \ . \tag{16}$$

For example, if the signal is recorded during $T = 10\,\mathrm{s}$, frequency resolution is equal to $\Delta f = 0.1\,\mathrm{Hz}$, thus inducing a speed error of $1\,\mathrm{m/s}$ to $2\,\mathrm{m/s}$ from the fundamental dominant excitation frequency $f_{c,1}$ calculation (depending on the carriage length). Of course, this error diminishes gradually with each harmonic however shorter recording times $T$ amplify this error. A solution is to pad the original signal with trailing zeros to a length sufficiently great to diminish the frequency resolution, but this reduces the signal energy meaning the precision of the dominant frequency method is diminished.

An elegant way to avoid these inaccuracies is to combine the ground vibration measurements with a numerical model to calculate the vehicle speed. However, the computational burden of existing models such as [3, 17, 18] complicates this approach, with excessive calculation times if the number of iterations is important. Despite this, as only the position of the dominant vehicle frequencies requires calculation, and amplitude magnitudes can be ignored, a simpler model can be suitable. Indeed, because the track/soil behaviour can be considered as linear elastic, the track/soil transmissibility is independent of the excitation amplitude and is defined by

$$H(f) = \frac{V_i(f)}{F(f)} \ , \tag{17}$$

where $F(f)$ is the vehicle excitation and $V_i(f)$ the ground vibration at a specific soil location. This relationship can be approximated by

$$|H(f)| = A(f)\mathrm{e}^{-\alpha f} \ . \tag{18}$$

According to Barkan's law [19], expressing frequency decay can be done using an exponential decay of constant $\alpha$, primarily due to material damping and its dependency on frequency. Amplitude $A$ depends on the distance from the track, and the vehicle, track and soil dynamic characteristics. Eventually, a simple expression of the ground vibration can be written as:

$$|V_i^{est}(f)| = |F(f)|A\mathrm{e}^{-\alpha f} \tag{19}$$

where $A$ is assumed to be independent of frequency and $F(f)$ is presented in the form of a series of Dirac functions representing the excitation coming from each wheelset

$$F(f) = P_{wheel}\,\mathrm{e}^{-j2\pi f t_k}\left(1+\mathrm{e}^{-j2\pi f(L_a/v_0)}\right)\left(1+\mathrm{e}^{-j2\pi f(L_b/v_0)}\right)\left(1+\sum_{i=1}^{n_c}\mathrm{e}^{-j2\pi i f(L_c/v_0)}\right) \tag{20}$$

with $n_c$ the number of carriages. This model is used because it is efficient and can be executed multiple times within a short time period. Although more advanced track/soil models are capable of higher prediction accuracy, this is not of concern. The fitting of the model to the experimental data can be performed in two steps:

1. First the model is fitted to the data in order to extract the decay rate $\alpha$, whilst ignoring vibration amplitude and vehicle speed.

2. Secondly a non-linear regression approach is used to determine $A$ and vehicle speed $v_0$; This is performed using the model parameters specified by Eqs. (19)–(20). The initial train speed value is calculated using the dominant frequency method.

Validation can be performed by comparing experimental spectra with the numerical solution of Eq. (19), as illustrated in Fig. 13. In this figure a theoretical curve has been calibrated to the experimental ground vibration spectrum in order to superimpose the dominant frequency peaks. The agreement between the two curves is not based on absolute amplitude criteria, but on the peak locations. It can be seen that these peak locations are determined with high precision as the fitting does not concentrate the maximum peaks but also around them.

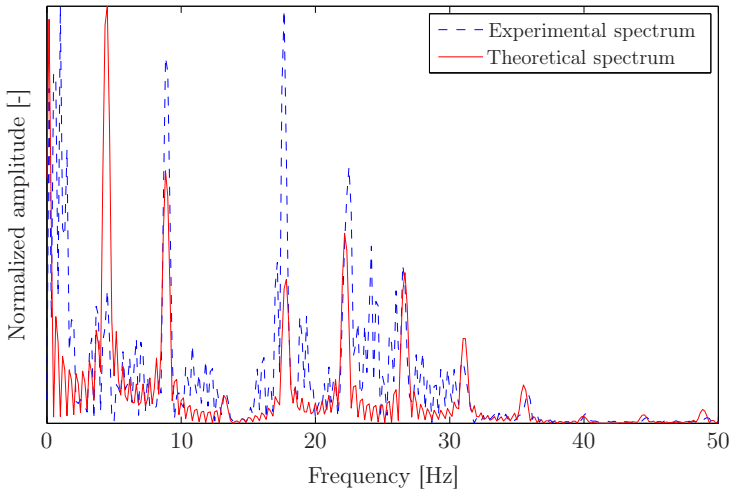


Figure 13: Comparison of the experimental and theoretical spectra after non-linear regression of the vehicle speed $v_0$

### 3.2 The use of multiple vibration sensors

Railway vibration experiments typically use an array of sensors to record vibration levels at different distances from the track. This creates a database of $m$ signals ($m$ is the number of sensors placed near the track). The aforementioned speed calculation procedure gives a set of $m$ values for the vehicle speed $v_0$.

During initial testing using the original dominant frequency method it was found that sensors placed at different distances from the track yielded different speed estimates, with some having a notable difference from the mean value. As a first step the average estimated speed from all sensors was calculated in order to reject outliers (occurrence indicator) and to calculate the mean value of $v_0$ from $l \leq m$ data. Using the developed procedures, $m$ train speed values are obtained and the use of the occurrence indicator is used to establish the final value of $v_0$. This average estimation naturally rejects the badly-estimated speed values outside a specified range and is especially very useful in the first estimations of vehicle speed.

### 3.3 Final disposition of the new calculation method

Figure 14 summarizes the newly proposed procedure with a focus on the enhancements made over original the dominant frequency method. Note that after each step, an occurrence analysis is performed to estimate the mean speed (if multiple ground vibration signals are used).

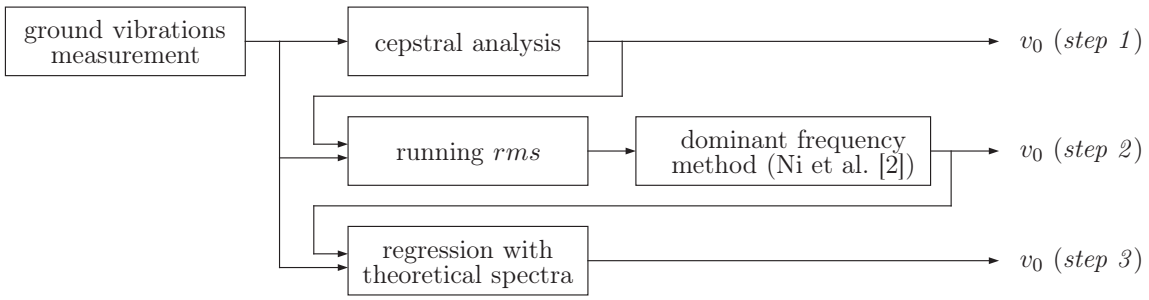


Figure 14: Chart of the automatic procedure for estimating the vehicle speed

The calculation method is based on the constant speed assumption. If the vehicle speed changes during acceleration or deceleration, the dominant frequencies changes over time.

## 4 Train speed calculator validation

### 4.1 Speed calculation using numerically predicted results

To numerically predict railway ground vibrations with high accuracy, Kouroussis et al. [20] presented and validated a prediction model based on a two-step approach (Fig. 15). This model was used to part-validate the new train speed calculation procedure.

This model was vastly different from the analytical model outlined in Section 3.1.3, because it facilitated a more detailed and accurate simulation of railway vibration. Previously it has been thoroughly validated against experimental field data and has been used to investigate various dynamic effects associated with vehicle speed [3, 21]. Despite this, it required much higher computational resources than the analytical model and the modelling approach was based on a two-step process. Firstly, the vibration of the vehicle/track/foundation subsystem was simulated, to obtain a time history of the forces exerted by the track and vehicle on the soil. Secondly, the track forces were used to excite the soil which was modelled using the finite element (FE) method. The model was capable of simulating vehicle dynamics in addition to complex soil geometries (for example, soil layering). Also, any kind of wheel and track unevenness was treated.

The first step was based on the philosophy adopted by the train constructor (multibody modelling). Although the rail was modelled with a discretely supported flexible beam, the other track parts were considered as lumped masses (sleepers, foundation) with interconnected elements (railpads, ballast). Ground wave propagation and velocity time histories were obtained via the second step using the FE soil model.

Using a numerical prediction model for speed calculation validation allowed for a high accuracy comparison because the vehicle speed was known. Moreover, a wide variety of train types, speeds and soil conditions could be tested. Depending on these conditions, the excitation mechanisms (e.g. quasi-static *vs* dynamic) may differ. Some generalisations for different train types

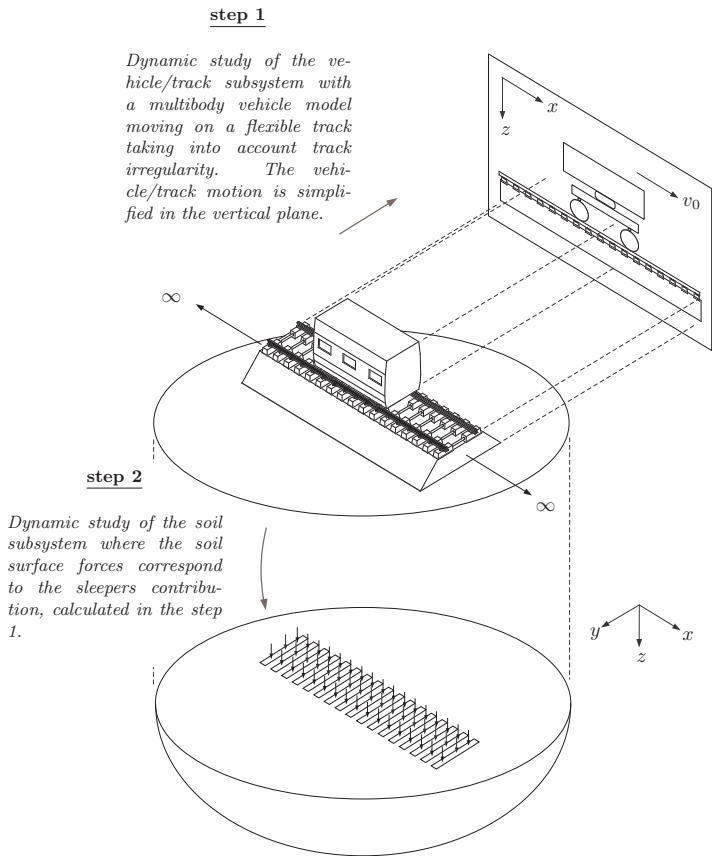


Figure 15: Description of the selected prediction model for ground vibration calculation [20]

can be made:

- High-speed trains are probably the most studied case in railway ground vibration. Quasi-static track deflection is the main contributor to the ground vibrations and high-speed lines are typically characterised by a very high quality of rolling surface.
- Urban networks (i.e. tramways) are characterised by a low speed and a relatively high density of singular rail surface defects like rail joints, rail crossings or an event such as gear switching. The dynamic track deflection mainly contributes to the ground wave generation.
- Domestic intercity trains travelling at moderate speed are often characterised by singular defects, with the quasi-static track deflection having a non-negligible influence on the ground vibrations. Therefore the excitation mechanisms are a combination of those experienced on high speed and urban railway lines.

### 4.1.1 Speed prediction for intercity and high-speed trains

Due to their similarities, the first two cases (intercity and high-speed trains) are briefly outlined. The main vehicle dimensions $L_c$, $L_b$ and $L_a$ are given in Fig. 16 and 17. The number $n_c$ of

passenger carriages is 8 for Thalys trains (locomotive and side carriage not included) and 12 for the intercity (IC) AM96 trains.

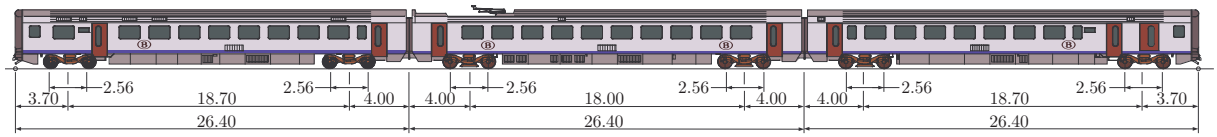


Figure 16: Configuration of the AM96 electric multiple unit

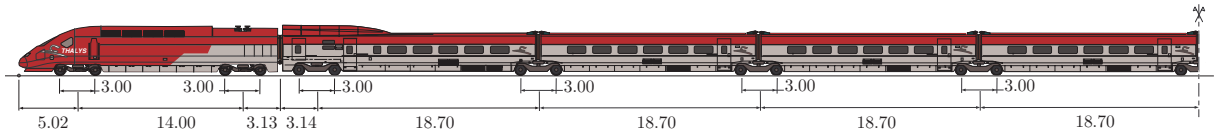


Figure 17: Thalys HST dimensions

The typical operational speed of the vehicles is 300 km/h for the Thalys and 115 km/h for the IC train. Therefore these speeds were used for the numerical simulations. Figure 18 gives the graphical results obtained using the dominant frequency method as originally presented by Ni et al. Cepstrum analysis has been used to estimate the initial vehicle speed (112.3 km/h for the IC train and 289.6 km/h for the HST) and the corresponding frequency range through Eq. (2). We observe that the peaks yield vehicle speeds close to their typical value but there are also several outliers. Generally, the higher harmonics provide more accurate results.

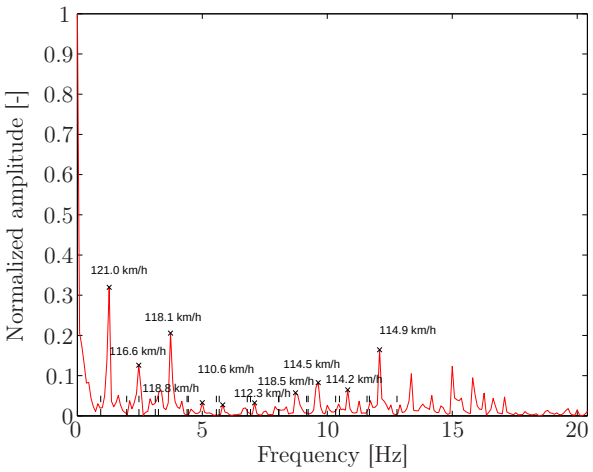


(a) AM96 intercity train running at 115 km/h

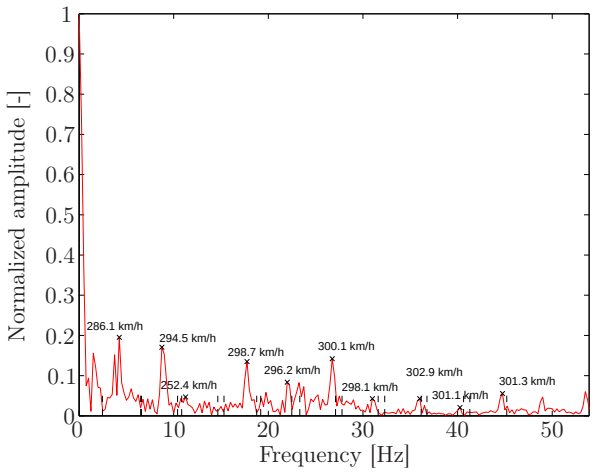


(b) Thalys HST running at 300 km/h

Figure 18: Ground vibration spectra and corresponding speed selection using dominant frequencies

By taking into account a sufficient number of virtual sensors along a profile perpendicular to the track and for the three directions $x$, $y$ and $z$, it is possible to observe the variation in train speed estimates with distance from the track and the direction of measurement (Fig. 19). Regarding distance from the track, results from near and far locations result in the same order of error. This is an important finding because it shows that speeds can be measured from large track

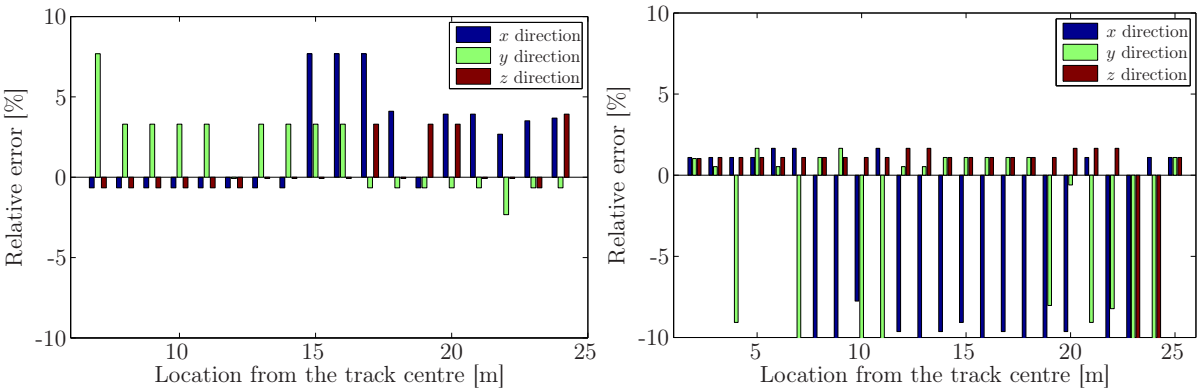


(a) AM96 intercity train running at 115 km/h (b) Thalys HST running at 300 km/h

Figure 19: Relative error of the original dominant frequency method as a function of vibration direction and distance from the track

offsets. This is advantageous for tracks with poor access, such as those constructed cuttings. In addition, it is noticed that vertical motions give better results.

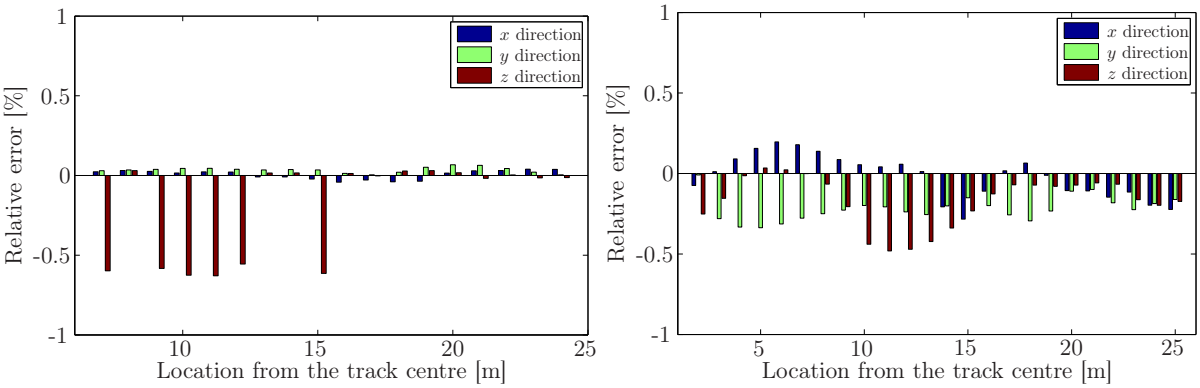


(a) AM96 intercity train running at 115 km/h (b) Thalys HST running at 300 km/h

Figure 20: Relative error of the newly proposed regression method as a function of vibration direction and distance from the track

Figure 20 shows the train speed estimation comparison, however this time the calculation has been aided using regression. A notable gain is achieved through the application of regression with relative error less than 1% and without particular correlation with the vibration direction.

### 4.1.2 Speed prediction for urban tramways

The train speed calculator was also tested against numerically predicted ground vibration data from a low speed T2000 tram. Figure 21 presents the geometrical configuration of this vehicle which had a low number of carriages ($n_c = 2$) in comparison to the intercity and high speed trains. The bogie axle distance was $L_a = 1.70\,\text{m}$ and the distance between the bogie was $L_b = 7.52\,\text{m}$. With a typical speed of 70 km/h, the dominant frequencies were reduced to a small frequency range. Two cases were studied depending on whether the singular defect was included on the

rail surface or not, in addition to an overall distributed unevenness.

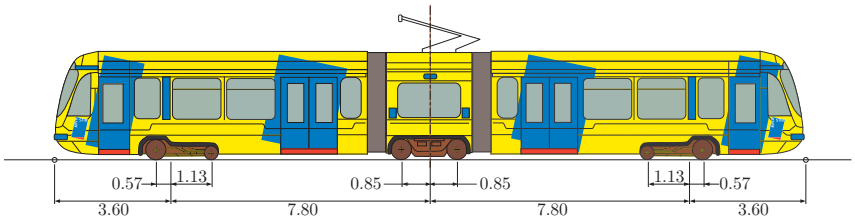


Figure 21: Configuration of the T2000 tram

Table 2: Speed evaluation in the case of the T2000 tram (speeds in km/h)

| Presence of a singular rail surface defect | | | | | | | | |
|---|---|---|---|---|---|---|---|---|
| Nominal speed | 10 | 20 | 30 | 40 | 50 | 60 | 70 | 80 |
| After cepstral analysis | 10.0 | 20.0 | 30.0 | 39.9 | 49.9 | 59.4 | 69.6 | 80.1 |
| After dominant frequency method | 9.6 | 20.0 | 30.1 | 38.9 | 51.0 | 60.5 | 68.4 | 81.2 |
| After regression | 9.6 | 20.2 | 30.4 | 38.0 | 50.7 | 61.1 | 71.2 | 81.0 |
| Absence of a singular rail surface defect | | | | | | | | |
| Nominal speed | 10 | 20 | 30 | 40 | 50 | 60 | 70 | 80 |
| After cepstral analysis | 10.1 | 20.4 | 30.5 | 40.4 | 50.8 | 60.5 | 71.2 | 81.4 |
| After dominant frequency method | 7.6 | 15.6 | 28.3 | 32.9 | 50.9 | 56.8 | 63.8 | 72.2 |
| After regression | 15.5 | 31.0 | 44.7 | 62.9 | 69.4 | 61.0 | 71.1 | 81.1 |

Table 2 summarizes the results obtained using cepstral analysis, the dominant frequency method and the regression method combined with the analytical function. The following observations were noteworthy:

- The presence of a singular rail surface defect amplified the each wheel passage effect, thus creating dominant peaks with strong amplitudes. The train speed estimates were of higher accuracy in the presence of defects in comparison to than those obtained without. This can be an important error in some cases.
- Similarly to the HST case, train speed did not significantly influence the accuracy of predictions. In the case of a singular defect, even very low speeds were accurately estimated.
- The dominant frequency and regression calculation procedures generated larger errors than the cepstral analysis procedure. There were two reasons for this finding. Firstly, the low tram speed meant that the dominant peaks were concentrated at very low frequencies. Secondly, in the absence of rail surface defects, quasi-static excitation was not dominant enough to generate high amplitude ground vibrations or a sufficient number of dominant frequency harmonics. This prohibited the use of the dominant frequency and regression calculation procedures.

## 4.2 Speed calculation using experimental field results on a high speed line

### 4.2.1 Measurement in Belgium

After validating the train speed prediction model against data obtained via numerical simulation it was tested against experimental data collected on commercial Belgian rail lines. Although numerical models are capable of predicting train vibration levels with accuracy, there will always be discrepancies between predicted vibration time histories and those recorded in-situ. This is due to the variety of modelling assumptions that underpin all numerical models. One discrepancy is that numerical models typically predict a more "idealised" signal, without the noise inherently associated with physical measurement. Therefore it was vital that the speed calculation tool could work with the noisy signals typically collected using vibration sensors.

Three Belgian test sites were investigated near the town of Leuze-en-Hainaut, Belgium for the purpose of analysing the effect of embankment conditions on high speed rail ground vibrations [22, 23]. These sites were chosen according to their track geometrical configuration: a track on an embankment, a track at-grade with respect to surrounding land and a track in cutting. Measurements close to an abutment were also made, for the embankment case (Fig. 22).

Figure 22: Abutment site

Many passages of HST were recorded during three days in August 2012, including the passing of Thalys HST, Eurostar HST and the French TGV. Uniaxial and triaxial geophone sensors (Sensor SM-6 low frequency) were used for site testing. Triaxial geophones were placed at distances between 9 and 35 m from the edge of closest rail, whereas the uniaxial grophones were placed up to 80 m from the rail. No method was used for determine the vehicle speed, however the approximate speed for all vehicles was 300 km/h (obtained from the train operator). Tables 3 to 6 present some vehicle speeds calculated using the new prediction methodology. For both 1-component (vertical direction) and 3-component vibration results it was found that all predicted speeds fell within a small range. The abutment case was also treated and was found to provide a reliable estimation of vehicle speed for each different sensor. Therefore it was concluded that the new speed evaluation method was applicable to any track/soil configuration. Figure 23 shows the relative error calculated from the final estimated speed for each vibration sensor, concluding that the distance from the track does not affect the quality of the result.

Table 3: Speed evaluation during the passing of HST's at the at-grade test site (26$^{th}$ August 2012)

| Train type | Track | Geophone setup | Time | Speed [km/h] |
|---|---|---|---|---|
| TGV | B (far) | 3 | 12:19 | 293.0 |
| Thalys | A (near) | 3 | 12:31 | 299.2 |
| Thalys | B (far) | 3 | 13:00 | 296.5 |
| Double Thalys | A (near) | 3 | 13:04 | 303.6 |
| Eurostar | B (far) | 3 | 13:45 | 292.2 |
| TGV | A (near) | 1 | 15:38 | 296.3 |
| Eurostar | A (near) | 3 | 16:16 | 300.5 |
| Double Thalys | B (far) | 1 | 16:27 | 295.8 |

Table 4: Speed evaluation during the passing of HST's on the embankment test site (27$^{th}$ August 2012)

| Train type | Track | Geophone setup | Time | Speed [km/h] |
|---|---|---|---|---|
| TGV | B (near) | 3 | 12:19 | 293.0 |
| Thalys | A (far) | 3 | 12:31 | 299.2 |
| TGV | A (far) | 3 | 12:39 | 299.4 |
| Thalys | B (near) | 3 | 12:59 | 296.5 |
| Eurostar | B (near) | 3 | 13:45 | 292.2 |
| Thalys | B (near) | 3 | 13:57 | 295.1 |
| TGV | A (far) | 1 | 15:41 | 296.6 |
| Eurostar | A (far) | 1 | 16:15 | 293.9 |

Table 5: Speed evaluation during the passing of HST's on the cutting test site (28$^{th}$ August 2012)

| Train type | Track | Geophone setup | Time | Speed [km/h] |
|---|---|---|---|---|
| Eurostar | A (far) | 3 | 11:13 | 296.9 |
| Thalys | B (near) | 3 | 11:22 | 297.0 |
| Eurostar | B (near) | 3 | 11:43 | 295.6 |
| TGV | A (far) | 3 | 12:40 | 298.9 |
| Thalys | A (far) | 1 | 15:36 | 281.3 |
| Eurostar | B (near) | 1 | 15:46 | 296.9 |

#### 4.2.2 Measurement in UK

High Speed 1 (HS1), also known as the Channel Tunnel Rail Link (CTRL), is a 108 km high-speed railway linking London, UK and Paris, France via the Channel Tunnel beneath the English Channel. Passages of Eurostar and Javelin HST's were recorded on 25$^{th}$ September 2012 – 27$^{th}$ September 2012 at three test sites close to Hollingbourne, UK. Site 1 had a cutting on one side (where measurements were taken) and an at-grade section on other (Fig. 24(a)). Site 2 was

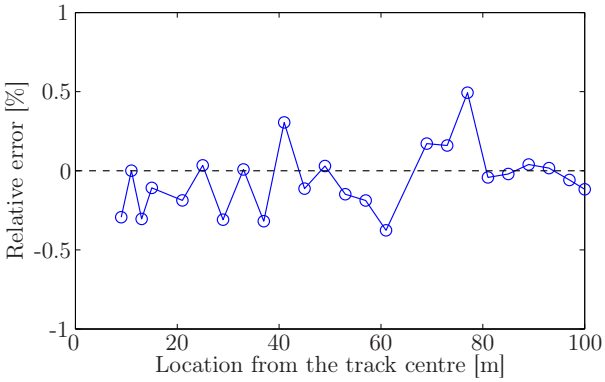


Figure 23: The effect of track distance on speed calculation on measured results

Table 6: Speed evaluation during the passing of HST's on the embankment and abutment test sites ($27^{th}$ August 2012)

| Train type | Track | Geophone setup | Time | Speed [km/h] |
|---|---|---|---|---|
| Thalys | A (far) | mixed | 18:32 | 298.2 |
| Double Thalys | A (far) | mixed | 18:33 | 297.9 |
| Eurostar | B (near) | mixed | 18:46 | 296.5 |
| TGV | B (near) | mixed | 19:37 | 295.3 |

situated above a "cut and cover" tunnel (Figure 24(b) was taken during its construction). Site 3 was an embankment (Fig. 24(c)). 3 component sensors were only placed on the embankment due to limited free field access.

(a) Site 1 (at grade and a cutting)

(b) Site 2 (above the tunnel)

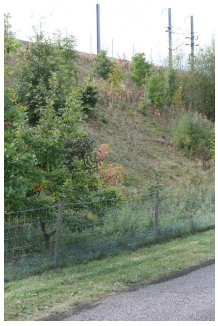

(c) Site 3 (embankment)

Figure 24: Three studied UK HST sites

The Javelin Class 395 is an electric multiple unit built in Japan by Hitachi for high speed commuter services on HS1. It is capable of running at a maximum speed of 225 km/h under overhead electrification on HS1, and 161 km/h on 750V DC third rail supply on conventional lines. Similarly to Thalys trains, two Javelings can be linked together. Therefore the basic 6-carriage train can be adapted to create a 12-carriage system. Javelin class 395 trains are

composed of intercity train carriages that have been upgraded to facilitate elevated speeds. Therefore more conventional bogies are used (for all carriages) in comparison to dedicated high speed bogies found in Thalys, TGV and Eurostar trains (Fig. 25). Unlike the aforementioned high speed trains, the Javelin carriage spacing ($L_c = 20\,\mathrm{m}$) is greater than the bogie spacing ($L_b = 14.17\,\mathrm{m}$). Therefore the excitation frequencies associated with $L_b$ and $L_c$ are different.

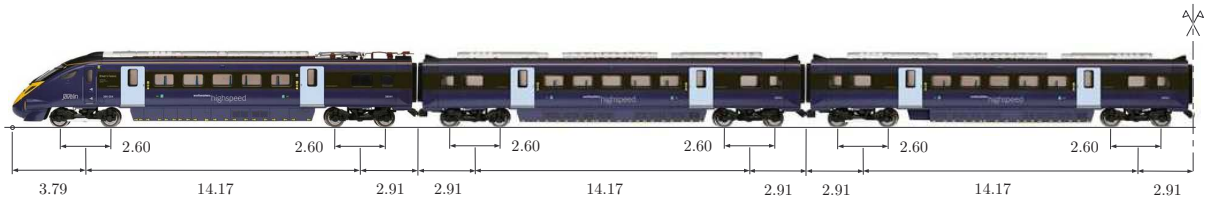


Figure 25: Javelin 395 HST dimensions

Tables 7 to 9 list the different passages recorded and the calculated vehicle speed, showing again the capabilities of the proposed estimation method to capture the vehicle speed for any track configuration, with or without the presence of complex structure in the vibration transmission path between the vehicle (source) and the sensors (receiver). Despite the high accuracy of prediction, the method has not been compared to speed estimates calculated using another reliable method.

Table 7: Speed evaluation during the passing of HST's on the high speed line HS1 in UK (at-grade track configuration)

| Train type | Track | Geophone setup | Time | Speed [km/h] |
|---|---|---|---|---|
| Eurostar | A (near) | 3 | 12:09 | 261.3 |
| Javelin 395 | B (far) | 3 | 12:42 | 216.2 |
| Javelin 395 | A (near) | 3 | 12:51 | 223.3 |
| Eurostar | A (near) | 3 | 13:11 | 290.3 |
| Javelin 395 | A (near) | 3 | 13:21 | 223.2 |

Table 8: Speed evaluation during the passing of HST's on the high speed line HS1 in UK (above the tunnel)

| Train type | Track | Geophone setup | Time | Speed [km/h] |
|---|---|---|---|---|
| Eurostar | A (near) | 3 | 11:52 | 266.4 |
| Javelin 395 | A (near) | 3 | 12:11 | 220.5 |

### 4.3 General remarks and discussion

The analysis of both experimental and numerical results revealed that the new method was more accurate than that proposed by Ni et al. [2]. Additional points of interest include:

Table 9: Speed evaluation during the passing of HST's on the high speed line HS1 in UK (embankment track configuration)

| Train type | Track | Geophone setup | Time | Speed [km/h] |
|---|---|---|---|---|
| Javelin 395 | B (near) | 3 | 12:30 | 211.1 |
| Eurostar | B (near) | 3 | 12:36 | 289.6 |
| Eurostar | A (far) | 3 | 12:52 | 283.2 |
| Javelin 395 | A (far) | 3 | 13:10 | 220.9 |
| Eurostar | A (far) | 3 | 13:23 | 288.2 |
| Javelin 395 | B (near) | 3 | 13:30 | 212.1 |
| Eurostar | B (near) | 3 | 13:40 | 268.6 |

- Railway-induced vibrations are generated by many physical mechanisms. Although the use of a numerical prediction model can simulate an array of variables and uncertainties that affect dominant frequencies, it was impossible to test every permutation of these variables. In this work, variations in axle load, vehicle dynamics, rolling stock geometrical parameters, track unevenness, track configuration, distance from the track and the soil characteristics were tested simulated and found not to degrade speed calculation accuracy. Despite this, some variables (and changes in variables) were not analysed (e.g. train weight changes due to passenger numbers, changes in track irregularities, and the presence of wheel flats). Regarding changes in train weight, this is unlikely to modify the frequency content of the signal, thus not affecting the prediction method. Regarding track irregularities, these are unlikely to affect speed prediction either because they mostly lie outside the range of frequencies used for speed analysis. Lastly, although wheel flats may have a quefrency similar to train wheel length, it is anticipated that they would not interfere drastically with the speed calculation because the cepstrum analysis utilises three separate rahmonics, thus minimising their effect.

- Background noise can contaminate the frequency spectrum of the vibrations generated from railways. Therefore the ability of the new calculation method to produce reliable results in the presence of such noise was investigated. To do so, a numerical normally distributed pseudorandom signal $v_{\text{noise}}$ was added to the recorded signals, to define the signal-to-noise ratio

$$SNR = \frac{\text{rms}(v_{\text{noise}})}{\text{rms}(v_{\text{signal}})} \tag{21}$$

  where $v_{\text{signal}}$ is the reference ground vibration velocity. Figure 26 presents the calculated relative error for a Thalys HST during at 300 km/h when $SNR$ varies. High accuracy is obtained after the regression analysis (and after the dominant frequency method application) even though results obtained after a cepstral analysis differ with greater $SNR$. This analysis gives a good picture of the model capability to tread the cases where the energy transmitted by the train pass-by (in particular, function of its weight) to the ground is not sufficient compared to the energy transmitted by other sources (car road, construction excitation,...).

- As the new procedure is frequency domain based, it is unable to calculate accelerations

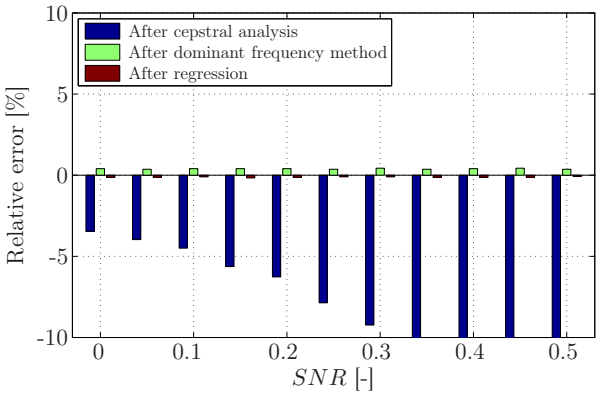


Figure 26: Relative error of the newly proposed method as a function of signal-to-noise ratio ($SNR$) for a Thalys HST running at 300 km/h

directly because it is based on a constant speed assumption. Despite this, it is possible to make a correct estimation of the speed means by treating only the vibration sensors close to the track (although sensor distance from the track does not affect velocity calculation, when considering accelerations, the closer the sensor is placed to the track the better it will respond). In the case of a constant acceleration, the train has a variable speed as calculated by the sensors which can be defined as

$$v(t) = v_0 + a_v\, t \tag{22}$$

where $a_v$ is the acceleration imposed to the vehicle. Speed $v_0$ is defined as the means of velocity in front of the virtual sensors placed along a perpendicular profile to the track: first wheelset run at a speed smaller (greater) than the one at last wheelset passing in front of sensors during acceleration (deceleration). Figure 27 shows the calculated speed after each evaluation step in the case of Thalys HST running around 300 km/h. The mean estimation after the final step (regression method) is clear between the maximum and minimum speeds during the train passage.

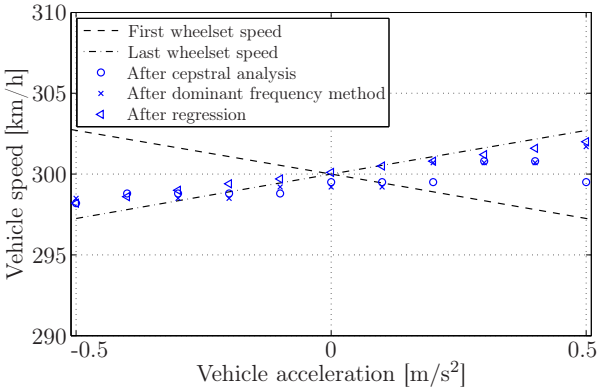


Figure 27: Vehicle speed estimation during deceleration/acceleration process for a Thalys HST running around 300 km/h

- The new method has been shown to provide reliable speed estimations up to large distances from the track (100 m — Fig. 23). Therefore it does not require direct track access meaning that under certain circumstances, it may serve as a preferable method to using wheel counters.

- Three speed estimation methods were proposed and the combined use of all three was found to increase prediction accuracy. The reason for this was that each method overcomes challenges inherent with the other two methods. Therefore this makes the overall technique suitable for all train types and speeds. Despite this, it is also possible to make an accurate assessment using only one of these methods (e.g. the tram case with the cepstral analysis). It should also be noted that cepstral analysis was a good choice for the initial speed estimation because it avoids divergence problems associated with the dominant frequency method.

- It should be noted that although the new calculation method was found to offer speed estimates with low deviation and a high correlation with both experimental and numerically generated velocity time histories, it was not compared to any speed estimates calculated using another reliable method.

## 5 Conclusion

A new method has been outlined to calculate train speeds on railway lines. The method uses a combination of cepstral analysis, dominant frequency methods and an analytical model combined with regression to calculate vehicle speeds. The new method can calculate speeds for any train type on any track/embankment arrangement. Additionally, it has high accuracy for sensors located up to 100 m from the track, thus allowing semi-remote, non-invasive monitoring of train velocities.

To show the robustness and ability of the proposed method to calculate a wide range of train speeds, it was used to predict speeds from numerically generated tram, intercity and high speed rail train passages with accuracy. Furthermore, to show its commercial applicability it was used to predict train speeds during field trials performed on operational railway lines in Belgium. The new method was shown to have offer high performance for several train types and track setups (including an abutment case). It was also compared to a commonly used alternative technique and shown to offer significant more accurate speed estimations. Furthermore, it was found to be applicable to a wider range of train speeds, train types and track configurations.

## Acknowledgement

The first author would like to acknowledge, Céline Crémer, Alexandre Mégret, Martin Courtois and Thibaut Hoet for their investigations into the dominant frequency method applicability, and Mehdi Scoubeau for his help during the ground vibration measurement in Belgium.

## References

[1] C. L. Ho, H. Huang, J. P. Hyslip, and S Chrismer. Field measurement of ground response of critical speed high speed trains on soft soil. In *12th International Railway Engineering Conference (Railway Engineering 2013)*, London (UK), 2013.

[2] S.-H. Ni, Y.-H. Huang, and K.-F. Lo. An automatic procedure for train speed evaluation by the dominant frequency method. *Computers and Geotechnics*, 38(4):416–422, 2011.

[3] G. Kouroussis, O. Verlinden, and C. Conti. Free field vibrations caused by high-speed lines: measurement and time domain simulation. *Soil Dynamics and Earthquake Engineering*, 31(4):692–707, 2011.

[4] X. Sheng, C. J. C. Jones, and D. J. Thompson. A comparison of a theoretical model for quasi-statically and dynamically induced environmental vibration from trains with measurements. *Journal of Sound and Vibration*, 267(3):621–635, 2003.

[5] L. Auersch. Ground vibration due to railway traffic — the calculation of the effects of moving static loads and their experimental verification. *Journal of Sound and Vibration*, 293(3–5):599–610, 2006.

[6] G. Lombaert and G. Degrande. Ground-borne vibration due to static and dynamic axle loads of intercity and high-speed trains. *Journal of Sound and Vibration*, 319(3-5):1036–1066, 2009.

[7] G. Kouroussis, C. Conti, and O. Verlinden. Experimental study of ground vibrations induced by Brussels IC/IR trains in their neighbourhood. *Mechanics & Industry*, 14(02):99–105, 2013.

[8] S.-H. Ju, H.-T. Lin, and J.-Y. Huang. Dominant frequencies of train-induced vibrations. *Journal of Sound and Vibration*, 319(1-2):247–259, 2009.

[9] J. Alias. *La Voie Ferrée — Technique de Construction et d'Entretien.* Eyrolles, Paris (France), 2nd edition, 1984.

[10] G. Kouroussis, O. Verlinden, and C. Conti. Influence of some vehicle and track parameters on the environmental vibrations induced by railway traffic. *Vehicle System Dynamics*, 50(4):619–639, 2012.

[11] G. Kouroussis, C. Conti, and O. Verlinden. Investigating the influence of soil properties on railway traffic vibration using a numerical model. *Vehicle System Dynamics*, 51(3):421–442, 2013.

[12] G. Lefeuve-Mesgouez, A. T. Peplow, and D. Le Houédec. Surface vibration due to a sequence of high speed moving harmonic rectangular loads. *Soil Dynamics and Earthquake Engineering*, 22(6):459–473, 2002.

[13] M. Heckl, G. Hauck, and R. Wettschureck. Structure-borne sound and vibration from rail traffic. *Journal of Sound and Vibration*, 193(1):175–184, 1996.

[14] T. Dahlberg. Railway track dynamics — a survey. Technical Report Railtrdy.doc/2003-11-06/td, Linköping University, 2003.

[15] A. V. Oppenheim and R. W. Schafer, editors. *Discrete-time signal processing*. Prentice Hall, New Jersey (USA), international edition, 1989.

[16] Deutsches Institut für Normung. *DIN 4150-2: Structural vibrations — Part 2: Human exposure to vibration in buildings*, 1999.

[17] D. Connolly, A. Giannopoulos, and M. Forde. Numerical modelling of ground borne vibrations from high speed rail lines on embankments. *Soil Dynamics and Earthquake Engineering*, 46:13–19, 2013.

[18] D. Connolly, A. Giannopoulos, W. Fan, P. K. Woodward, and M.C. Forde. Optimising low acoustic impedance back-fill material wave barrier dimensions to shield structures from ground borne high speed rail vibrations. *Construction and Building Materials*, 44:557–564, 2013.

[19] D. D. Barkan. *Dynamics of Bass and Foundations*. McGraw — Hill Book Company, New York (USA), 1962.

[20] G. Kouroussis, O. Verlinden, and C. Conti. A two–step time simulation of ground vibrations induced by the railway traffic. *Proc. IMechE, Part C: Journal of Mechanical Engineering Science*, 226(2):454–472, 2012.

[21] G. Kouroussis, O. Verlinden, and C. Conti. Efficiency of resilient wheels on the alleviation of railway ground vibrations. *Proc. IMechE, Part F: Journal of Rail and Rapid Transit*, 226(4):381–396, 2012.

[22] G. Kouroussis, D. Connolly, M. Forde, and O. Verlinden. An experimental study of embankment conditions on high-speed railway ground vibrations. In *20th International Congress on Sound and Vibration (ICSV19)*, Bangkok (Thailand), 2013.

[23] D. P. Connolly, G. Kouroussis, W. Fan, M. Percival, A. Giannopoulos, P.K. Woodward, O. Verlinden, and M. C. Forde. An experimental analysis of embankment vibrations due to high speed rail. In *12th International Railway Engineering Conference (Railway Engineering 2013)*, London (UK), 2013.